A damage energy criterion for cohesive zone model

André Chrysochoos, Loïc Daridon, Mathieu Renouf

A damage energy criterion for cohesive zone model

A. Chrysochoos[a,b], L. Daridon[a,b,*], M. Renouf[a,b]

[a] *LMGC, Université de Montpellier, CNRS, Montpellier, France*
[b] *MIST, Université de Montpellier, IRSN, CNRS, France*

Abstract

The objective of this paper is to present an energy damage criterion for cohesive zone models (CZM) within the framework of the non-linear thermodynamics of irreversible processes (TIP). An isotropic elastic damageable material is considered for isothermal transformations. Damage is then the only irreversible effect accompanying the deformation process and this mechanism is supposed to be fully dissipative. Once a separation law and a damage state variable have been chosen, the paper shows that the damage criterion can be automatically derived from the energy balance. From this observation, a CZM is derived for a given choice of traction-separation law and damage state variable and the quality of its numerical predictions is analyzed using an experimental benchmark bending test extracted from literature. Finally, damage, elastic and dissipated energy fields around the crack path are shown during this rupture test.

Keywords: cohesive zone, damage, fracture, thermodynamics of irreversible processes, energy balance, Finite element analysis

∗. Corresponding author
Email addresses: andre.chrysochoos@umontpellier.fr (A. Chrysochoos), loic.daridon@umontpellier.fr (L. Daridon), mathieu.renouf@umontpellier.fr (M. Renouf)

1. Introduction

In many engineering applications, the fracture behavior of the structure is crucial, which is why damage mechanisms have been studied over the last decades, from a theoretical, numerical and experimental point of view, using different frameworks [5; 46]. Since the pioneering work of L. M. Kachanov [39], continuum damage mechanics has become a scientific discipline focusing on the effects of various microdefects on the macroscopic behavior of materials and structures. Macroscopic damage descriptions often use a damage variable which is linked to loss of stiffness [15; 43]. For a given elastic material, the stiffness tensor $\mathbf{E_d}$ at a certain level of isotropic damage, denoted by d, is very often related to the stiffness tensor $\mathbf{E_0}$ of the undamaged material as follows : $\mathbf{E_d} = (1-d)\mathbf{E_0}$. In the particular case of the Thermodynamics irreversible Processes (TIP) framework [6], the elastic free energy of damageable material, ψ, is also defined in the same way $\psi = (1-d)\psi_0$, where ψ_0 is the elastic free energy of the non damaged material. The conjugate variable associated with the damage state variable, d, is by definition $Y_d = \frac{\partial \psi}{\partial d}$, leading to a thermodynamic force X_d which is given by $X_d = -Y_d = \psi_0$, the elastic energy of the undamaged material. Classically, for material behavior using threshold criterion, the thermodynamic force X_d is then used to define the damage rate $\dot{d}$, through a yield function F and its associated flow rule [21; 46].

An alternative numerical strategy to predict the evolution of damage and crack propagation is to introduce a $2D$ cohesive zone model (CZM) between two elastic layers. The CZM model is considered as a zero-thickness medium where the traction-separation law can be derived from a surface's free energy. This numerical approach has been widely used in many areas of

computational mechanics [4; 22; 23; 25; 53; 54; 69]. Indeed the fracture of concrete and the delamination of composites are some important examples of application areas of damage mechanics. To model elastic damageable materials, the main assumption is that all the damage that occurs in the bulk are gathered in a cohesive zone. In a finite element approach the cohesive zone is then located between two elements where elastic behavior remains linear [9]. Since the pioneering works carried out by Dugdale and Barenblatt [7; 29], many cohesive-zone models were proposed in the literature [17; 22; 23; 33; 34; 72; 73]. Cohesive-zone models taking fatigue into account were developed to simulate crack propagation under cyclic loading conditions [55; 66] while others were developed to combine two irreversible phenomena such as damage and plasticity [42]. The identification of CZM requires the coupling of experimental data and numerical studies to accurately define the traction separation law [10; 20; 35; 40; 41; 64].

A classic criticism of the cohesive zone methods is their relative dependency on mesh size. For example, intrinsic CZM approach for crack propagation has a deficiency of introducing artificial compliance to the model and crack path dependency because the cohesive elements are inserted between every 2D or 3D elements [38; 67; 74]. To remedy this mesh dependency, associated with the vanishing of stiffness, a new class of so-called "non-local methods" has appeared in the domains of damage and fracture mechanics. Two main regularization techniques exist to avoid pathological localization, namely the integral [63] or the gradient [5; 47; 61] damage approaches. Both consist in introducing non-local terms in the formulae of the cohesive model

associated with a characteristic length. For example, in the Thick Level Set method, which is an integral damage approach, the undamaged zone is separated from the totally damaged zone by a level set [50; 51]. The damage variable is then an explicit function of the level set. The damage growth in solids is based on the movement of a layer of finite thickness l_c within which the damage varies continuously. Then, the damage rate is directly linked to the set propagation. The non-local aspect of this method is essentially due to the fact that the configurational force driving the damage front is an average value over the thickness of the level set in the wake of the front [8; 45]. As in bulk damage mechanics, this approach allows the cracks' initiation and propagation within the same framework.

Another way to regularize the damage progress is to add a gradient-dependent term and to derive the problem of damage evolution from a variational approach based on an energy formulation [48]. This approach has also been used to couple the models for gradient-damage and those for plasticity [2; 3] or to develop a cohesive zone model suitable for fatigue fracture [1; 13; 62]. The macroscopic behavior can be seen as brittle fracture with a Griffith-like criterion associated with cohesive fracture of the Barenblatt or Dugdale types [24; 62]. The variational formulation of fracture mechanics framework has also been used to develop the Eigen-erosion scheme [58; 59]. In this finite element approximation scheme, the crack tracking problem is done by successively eroding elements when the attendant elastic energy releaseable exceeds the critical fracture energy.

The objective of the following sections is to construct an energy damage criterion for an isotropic elastic damageable material within the TIP framework. The construction of the CZM is performed under the small strain hypothesis. The damage law is based on the premise that the damage progress is linked to a prescribed evolution in the maximum elastic energy that can be stored within the material for a given damage state. The damage mechanisms are the only microstructural irreversible effects accompanying the deformation processes and these mechanisms are fully dissipative (no energy storage is induced by the material degradation). Naturally, damage dissipation may induce self heating leading to non-isothermal deformation processes that are consequently irreversible due to heat diffusion. However for sake of simplicity, only isothermal transformations are considered and the chosen state variables are the displacement jump $\mathbf{u}$ and a scalar damage variable, denoted by u_d. The damage variable u_d can be related to the effective displacement as used in [9; 25; 26; 60]. The 2D cohesive zone model proposed in this paper is constructed this way.

The layout of the paper is as follows. The energy criterion of the damageable elastic cohesive zone model is presented in Section 2 through a 1D scenario within the TIP framework. In Section 3, a vectorial extension of the cohesive zone law is proposed for an isotropic damage evolution. In Section 4, the capability of the model is investigated using an experimental benchmark test (i.e. a single-edge notch-bending specimen for fracture toughness testing) [31; 50; 51; 70]. Mechanical and energy responses are shown and discussed. In particular, several damage, elastic and dissipated energy fields around the

fracture paths are plotted during the crack propagation. The computation of the dissipated energy fields is of special interest inasmuch as they can be compared with the ones derived from quantitative IR techniques [18].

2. 1D scenario

The objective of the following section is to briefly review the mechanical concepts classically introduced with CZM in the case of a 1D monotonic traction and to embed them into the TIP framework to derive, through an energy criterion, a damage evolution law.

2.1. Mechanical aspects

In the literature [12], the mechanical response of the cohesive zone is described by the correspondence between the " normal traction" force f supported by the interface and its normal opening displacement often called "separation" during a monotonic opening. Depending on the chosen form of the traction-separation diagram, the relationships are called bilinear, polynomial or exponential cohesive laws. In Figure 1 a polynomial form has been chosen to illustrate the most commonly characteristics of these curves. We find the cohesive strength f_0 corresponding to the maximum of the traction–separation curve or its associated opening displacement u_0, the maximum value of separation u_c corresponding to the crack opening. An energy parameter is also often mentioned [57] : this is the fracture energy $A_c = \int_0^{u_c} f(u)du$ (work of separation), which is the area below the traction-separation curve.

This traction-separation curve is considered as a threshold over which the damage develops irreversibly. This threshold is an intrinsic characteristic of

the cohesive zone behavior. When unloading is considered, it is supposed to be purely elastic, assuming that the damage progress stops as soon as the loading point is below the threshold curve. For convenience, the elastic unloading paths are often directed towards the origin of the traction–separation diagram (see Figure 1). This implies that the elasticity remains linear and that there is no residual opening at the end of the unloading.

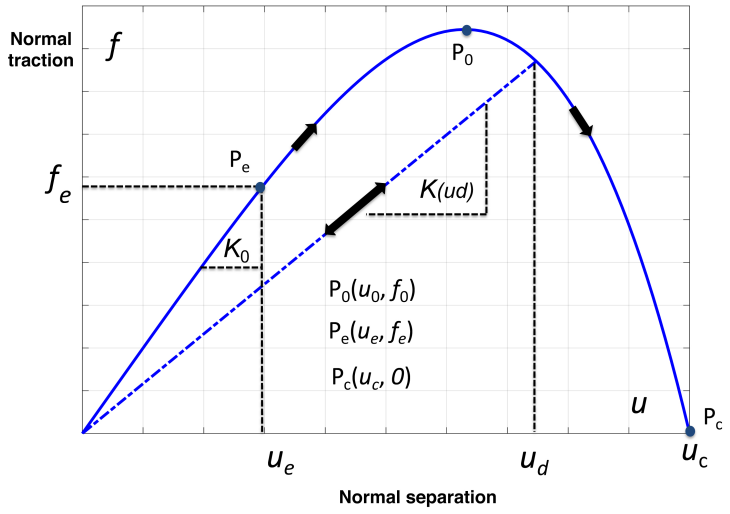

FIGURE 1: Traction-separation diagram. Monotonic envelope (continuous line), elastic unload or reload (dashed line). An arbitrary polynomial cohesive law has been chosen.

The progress of the damage can be depicted by a continuous decrease of the secant stiffness $K = \frac{f}{u}$ towards zero until rupture at u_c . A classical scalar definition of the damage variable can then be given by :

$$D_k = \frac{K_0 - K}{K_0} \ , \tag{1}$$

where K_0 is the initial stiffness of the cohesive zone [11]. The variable D_k

progressively increases from 0 to 1 when the opening displacement increases from 0 to u_c (or from u_e to u_c when a pure elastic domain, $[0, u_e]$, is introduced in the traction-separation curve (see Figure 1)).

A second possibility is to consider a normalized deformation energy definition of the damage [57] :

$$D_A = \frac{A}{A_c}, \text{ where } A = \int_0^u f(\upsilon) d\upsilon \ . \tag{2}$$

Here again, this last definition slightly changes when an elastic domain limited by the point (u_e, f_e) is introduced. In such a case, *Eq.*(2) requires a renormalization :

$$D_A^* = \frac{A^*}{A_c^*}, \text{ where } A^* = \int_{u_e}^u f(\upsilon) d\upsilon \text{ and } A_c^* = \int_{u_e}^{u_c} f(\upsilon) d\upsilon \ . \tag{3}$$

Then by construction D_A and D_A^* belong to $[0, 1]$. In fact, there are many ways to define damage. The damage process being assumed irreversible, the damage variable rate is often chosen to be non-negative whatever the loading history, to depict its monotonic evolution. Damage develops when the mechanical state (u, f) corresponds to a point of the cohesive threshold curve. In what follows we have chosen a kinematic definition of the damage variable. Like previously done by numerous authors (*e.g.* [68]), we have chosen the maximum value of the separation u_d ever reached by the cohesive zone until instant t. This damage variable is then defined at instant t by :

$$u_d = \max \{u(\tau), \forall \tau \leqq t\} \ . \tag{4}$$

This variable monotonically increases during the damage progress from 0 to u_c whatever the loading path (see Fig.1)) .

2.2. Energy aspects

Usually during a load cycle, the deformation energy w_{def}, which corresponds to the area surrounded by the loading curve *Eq.*(7) is transformed into dissipated energy, denoted by w_d, and stored energy, denoted by w_s, due to the irreversible microstructural transformations accompanying the deformation process. Part of w_{def} can also involve strong thermomechanical coupling energy (heat) w_{thm} [19]. An illustrative example of the coupling effects on the mechanical response can be given by the famous thermoelastic damping presented by Zener in [71]. The general form of the energy balance over a loading cycle can then be written as :

$$w_{def} = w_d + w_s + w_{thm} \ . \tag{5}$$

For any other loading the elastic energy, w_e, has to be added so that :

$$w_{def} = w_e + w_d + w_s + w_{thm} \ , \tag{6}$$

w_e vanishing, by construction, over a loading cycle. In the present situation, we only consider isothermal transformations with no thermomechanical coupling. Moreover, we assume that damage is a pure dissipative mechanism and that, consequently, no energy storage or release of stored energy, due to microstructural changes, occurs during the loading. These assumptions imply $w_s = 0$ and $w_{thm} = 0$.

For any kind of separation-controlled loading $\{u(\tau), \forall \tau \leqq t\}$, the deformation energy at instant t is here defined by :

$$w_{def}(t) = \int_0^t f(\tau)\dot{u}(\tau)d\tau \ . \tag{7}$$

For monotonic loadings, the mechanical state follows the traction-separation curve. The deformation energy then represents the mechanical energy required to reach the damage state $u_d = u(t)$. This cost in deformation energy can be defined by :

$$w^d_{def}(u_d) = \int_0^{u_d} f(\upsilon) d\upsilon \ . \tag{8}$$

Another important mechanical energy term is the elastic energy, $w_e(u, u_d)$, in the cohesive zone at a given state of damage u_d. It is defined by :

$$w_e(u, u_d) = \frac{1}{2} K(u_d) u^2 \ . \tag{9}$$

Note that this energy is mechanically recoverable during the unloading. This is the reason why it did not appeare in the general form of the energy balance proposed in *Eq.*(5) for a complete loading cycle.

As previously done for the deformation energy during monotonic loading, we can define the elastic energy $w^d_e(u_d)$ by :

$$w^d_e(u_d) = \frac{1}{2} K(u_d) u_d^2 = w_e(u_d, u_d) \ , \tag{10}$$

which represents the maximum elastic energy mechanically recoverable for a given damage state, defined by u_d.

As previously supposed (no thermomechanical coupling energy, no energy storage) the difference between $w^d_{def}(u_d)$ and $w^d_e(u_d)$ is attributed to the energy dissipation accompanying the irreversibility of damage mechanisms. We can then define the dissipated energy by $w^d_d(u_d)$:

$$w^d_d(u_d) = w^d_{def}(u_d) \ - \ w^d_e(u_d) \ , \tag{11}$$

210 $w_d^d(u_d)$, $w_e^d(u_d)$ and $w_{def}^d(u_d)$ are illustrated in Figure 2.

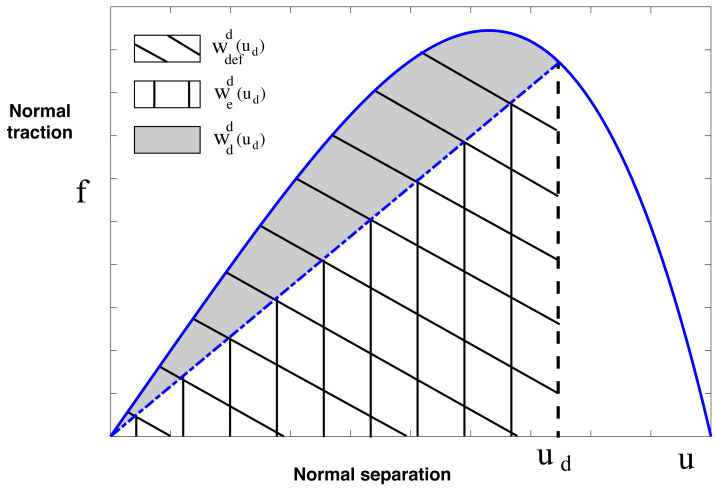

FIGURE 2: Energy illustration of the traction-separation diagram. Monotonic envelope (continuous blue line), elastic unload (dashed blue line).

211 Based on the mechanical response chosen in Figure 1, the evolutions of
212 the three different energies associated with a loading-unloading tensile testing
213 are shown in Figure 3. The deformation, elastic, and dissipated energies are
214 plotted in green, blue, and red respectively. The deformation energy w_{def} is
215 naturally the sum of the dissipated w_d and elastic w_e energies *Eq.*(6) since
216 the damage is supposed to be the only microstructural transformation which
217 is fully dissipative during loading, see *Eq.*(11) (no energy storage is induced
218 by the microstructural transformations). Figure 3a illustrates that during
219 the elastic unloading w_e^d remains constant (no evolution of damage) while w_e
220 returns to zero. In parallel, the deformation energy w_{def} also decreases and
221 tends towards the energy previously dissipated during the first loading cycle,
222 w_d^d. In Figure 3b the elastic reloading while $u \leq u_d$ is shown (dashed lines)
223 and extended by a monotonic loading until rupture for $u_d = u_c$ (full lines).

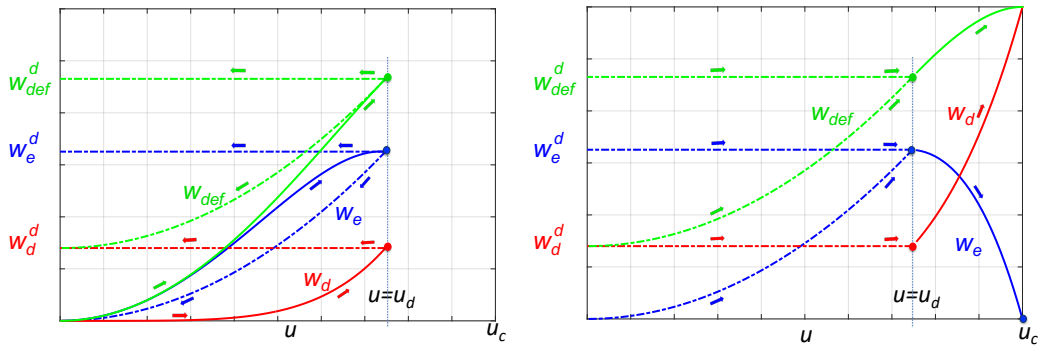

(a) Loading up to $u = u_d$ and unloading. (b) Reloading until rupture.

FIGURE 3: Energy balance evolution during a load-unload-reload process - Continuous lines are associated with the monotonic envelope, dashed lines correspond to the elastic unload and reload.

Under these restrictive assumptions, the area under the traction-separation curve, Figure 1 (equivalent to a monotonic traction rupture) is completely dissipated when the cohesive zone vanishes. In the next sub-section once the thermodynamic working framework has been specified, this important property is discussed. Then, another point to underline is that if the traction-separation curve is classically considered as the constituent element of the behavior of the cohesion zone, it is thus the same for the evolutions of $w^d_{def}(u_d)$ and $w^d_e(u_d)$. Therefore, instead of using the tension-separation curve to describe the damage progress, associated with the loss of stiffness, it is also possible to use the evolution of the allowable maximum elastic energy w^d_e to define the threshold function associated with the damage rate.

2.3. Thermodynamics aspects

In this sub-section, we propose to integrate the above results and comments into the TIP framework.

2.3.1. Cohesive zone potential and state laws

In the case of isothermal transformations, the chosen state variables are (u, u_d). A first gambling of the thermomechanical approach is to assume the existence of a potential $\psi(u, u_d)$ capable of gathering all the state laws. Here we identify this potential to the elastic energy w_e defined in *Eq.*(10) :

$$\psi(u, u_d) = \frac{1}{2} K(u_d) u^2 \ . \tag{12}$$

The state laws are by construction the partial derivatives of the potential with respect to the state variables. We then define the conjugate variable f^r, associated with u which represents the reversible part of the traction force, and A_d associated u_d respectively :

$$\left\{ \begin{array}{rcccl} f^r & = & \frac{\partial \psi}{\partial u} & = & K(u_d) u \\ A_d & = & \frac{\partial \psi}{\partial u_d} & = & \frac{1}{2} K'(u_d) u^2 \end{array} \right. , \tag{13}$$

where $K'(u_d) = \frac{\mathrm{d}K(u_d)}{\mathrm{d}u_d}$.

2.3.2. Clausius-Duhem inequality

The irreversibility of the mechanisms accompanying the opening of the cohesive zone is depicted by the Clausius-Duhem inequality which enables the definition of the intrinsic dissipation w_d^o . In the present framework, it can be written as :

$$w_d^o = w_{def}^o - \dot{\psi} = f\dot{u} - \frac{\partial \psi}{\partial u}\dot{u} - \frac{\partial \psi}{\partial u_d}\dot{u_d} = f^{ir}\dot{u} + X_d \dot{u_d} \geq 0 \ . \tag{14}$$

The terms w_d^o and w_{def}^o determine the dissipated and deformation energy rates, respectively. The symbol $(-)^o$ is introduced to underline that w_d and w_{def} are not a priori state functions and are then path dependent. *Eq.*(14) also introduce the irreversible part of the traction force, $f^{ir} = f - f^r$, and the thermodynamic force X_d associated with $\dot{u_d}$. Note that during an irreversible transformation $\dot{u_d} > 0$ we get $X_d = -A_d$. If damage is the only irreversible process, no dissipation has to be associated with $\dot{u}$. In such a case the irreversible traction force vanishes $f^{ir} = 0$. The traction force f can then be directly defined via the state law :

$$f \; = \; f^r \; = \; K(u_d)u \; . \tag{15}$$

Moreover, the intrinsic dissipation becomes with Eqs (13) and (14) :

$$w_d^o = X_d \dot{u_d} = -\frac{1}{2} K'(u_d) u^2 \dot{u_d} \geq 0 \; . \tag{16}$$

The fact that $\dot{u_d} \geq 0$ implies $K'(u_d) \leq 0$ what is physically consistent. The irreversible nature of damage leads to a degradation of the secant stiffness.

2.3.3. Threshold function and damage evolution law

In the TIP framework the thermodynamic forces are supposed to be function of the state variable rates. In the case of the linear TIP proposed by Onsager [56], the correspondence between thermodynamic forces and state variable fluxes is linear. The Onsager's matrix is supposed to be symmetric positive definite in order to verify the Clausius-Duhem inequality (positive dissipation) whatever the thermodynamic process. Extension to non-linear

theory exists as for example the formalism of Generalized Standard Materials [6]. Based on the hypothesis of normal dissipation, the thermodynamic forces derive from a convex dissipation potential or equivalently, state variables rates derived from a dual dissipation potential, function of the thermodynamic forces. This dissipation potential can also involve the state variables of the model as parameters. This last option is referred to as non-associated behavior [46]. For threshold laws (e.g. in plasticity), these options are often chosen. A common approach is then :

- to define a threshold function depending on the thermodynamic forces (and possibly state variables)
- to write that irreversibility occurs and develops if the thermodynamic state is on the threshold and remains on it during a time increment.

Note that once the state laws (derived from the thermodynamic potential) and complementary laws (derived from the dissipation potential) have been written, it is then possible to deduce the evolution of the energy balance associated with the transformation.

In what follows in as much as our approach is directly based on the energy balance form imposing by construction non-negative dissipation, the existence of the threshold function will not be associated with the normal dissipation hypothesis. Indeed, the current elastic domain is characterized by $w_e^d(u_d)$ the maximum elastic energy available for a given damage state which also corresponds to the energy required to further damage the material. Then we have :

$$w_e(u, u_d) \leq w_e^d(u_d) \ . \tag{17}$$

The evolution law for u_d is then derived from the fact that for the damage to occur the maximum elastic energy allowable in the material has to be and remain on the threshold during the loading step, i.e.

$$\left\{ \begin{array}{rcll} w_e(u,u_d) & = & w_e^d(u_d) & \text{(a)} \\ \dot{w}_e(u,u_d) & = & \dot{w}_e^d(u_d) & \text{(b)} \end{array} \right. . \tag{18}$$

The first equality gives naturally $u_d = u$. The second equality leads to a proposal of evolution equation for the damage :

$$\dot{u}_d = \left\{ \begin{array}{llllll} \dot{u} & \text{if} & u = u_d & \text{and} & \dot{u} \geq 0 \\ 0 & \text{if} & u < u_d & \text{or} & \dot{u} \leq 0 \end{array} \right. , \tag{19}$$

what is consistent if we remind the definition of the damage state variable *Eq.*(4) and the fact that the damage increases irreversibly, $\dot{u}_d \geq 0$.

To be fully compatible with non-linear TIP framework, the final step is to propose a threshold function that takes the thermodynamic force X_d into account. As previously stated, we consider a derivative form of the energy balance to get this threshold function *Eq.*(18)b. By using *Eq.*(13) and *Eq.*(16), we get :

$$\frac{d\, w_e}{dt} = -X_d\, \dot{u}_d + K(u_d) u\, \dot{u} \ . \tag{20}$$

On the threshold, *Eq.*(20) becomes :

$$\frac{d\, w_e^d}{d\, u_d} \dot{u}_d = (-X_d + K(u_d) u_d)\ \dot{u}_d \ . \tag{21}$$

Then a threshold function F involving the thermodynamic force X_d and the state variables can be taken under the form :

$$F(X_d; u, u_d) = K(u_d)u - X_d - \frac{d\, w_e^d}{d\, u_d} \ . \tag{22}$$

To be consistent with the incremental form of the energy balance, the equality $F(X_d; u, u_d) = 0$, gives once again $u_d = u$ while the consistency condition $dF = 0$ leads to $du = du_d$, or equivalently to *Eq.*(19).

To be precise, the full calculation of $dF = 0$ at $u = u_d$ leads to :

$$(K(u_d) + 2\, K'(u_d)u_d)\, (du - du_d) = 0 \ , \tag{23}$$

then $du = du_d$, except possibly when $u_d = -\frac{K(u_d)}{2\, K'(u_d)}$.

2.3.4. Some comments about the damage evolution equations

To depict the evolution of damage, in addition to the traction-separation curve data, the literature often proposes a specific evolution equation in the form of $\dot{D} = \dot{D}(f, D, \dot{u})$ whatever the definition of the damage variable D [11; 44; 65].

In the foregoing, because of the hypotheses explicitly made on the energy balance (i.e. damage is the only dissipative mechanism and it is totally dissipative), the damage evolution law is fixed by the definition of the damage variable itself and by the explicit form of the energy balance. With the chosen definition of the damage variable given in *Eq.*(4), we derive an evolution equation given in *Eq.*(18), which is an extremely simple form of the general equation proposed by [65].

Another evolution equation could lead, in our case, to no longer respect the properties of the energy balance as first assumed. The consequences could be the appearance of energy storage mechanisms, i.e. $\dot{w}_d^d < \dot{w}_{def}^d - \dot{w}_e^d$,

or internal energy transformation into dissipated energy (release of stored energy), i.e. $\dot{w}_d^d > \dot{w}_{def}^d - \dot{w}_e^d$. Taking this stored energy variations should lead to the introduction of new internal state variables and/or to a change of the deformation energy rate definition [30].

3. 2D cohesive zone model

In this paragraph, we propose an extension to a vectorial version of the CZM where the isotropic damage is controlled by the evolution of the maximum storable elastic energy. Isotropic damage means here that a scalar state variable is solely used to describe the damage evolution. This generalization has been made by following the same approach as the one previously proposed.

3.1. Mechanical variables

Regarding the mechanical description of the cohesive zone, the traction force and the separation become now vectors. Let us introduce a frame of reference where directions 1 and 2 correspond to the tangent plane of the cohesive zone while direction 3, is the normal direction. The traction vector, $\mathbf{f}$, whose components are (f_{t_1}, f_{t_2}, f_n) and the separation vector, $\mathbf{u}$, which has 3 components denoted by (u_{t_1}, u_{t_2}, u_n) are introduced. As is conventionally admitted in CZM, the normal move jump denoted by u_n is positive or null. For a long time, this unilateral condition has been taken into account by a Signori relation in numerical simulations performed with the software program, LMGc90 [27].

338 *3.2. Cohesive zone potential and state equations*

Before defining the cohesive zone potential that is a state function, a set of state variables has to be chosen. Here we selected the components (u_{t_1}, u_{t_2}, u_n) of the separation vector and a scalar damage variable denoted by u_d. Then, to generalize the form of the cohesive zone potential proposed in *Eq.*(12), the following form, inspired by [11], is adopted :

$$\begin{array}{rcl} \psi(\mathbf{u}, u_d) & = & w_e(\mathbf{u}, u_d) \\ & = & \frac{1}{2}\left(K_n(u_d)u_n^2 + K_t(u_d)u_{t_1}^2 + K_t(u_d)u_{t_2}^2\right) \\ & = & \frac{1}{2}K_n(u_d)(u_n^2 + \alpha u_{t_1}^2 + \alpha u_{t_2}^2) \\ & = & \frac{1}{2}K_n(u_d)u_{eq}^2 \end{array} \quad , \tag{24}$$

where :

$$u_{eq} = (u_n^2 + \alpha u_{t_1}^2 + \alpha u_{t_2}^2)^{\frac{1}{2}} \ . \tag{25}$$

339 The variable α is the ratio between $K_t(u_d)$, the tangential and $K_n(u_d)$,
340 the normal secant stiffnesses at a given u_d. In the case of isotropic damage α
341 is a constant.

342 In *Eq.*(26), a 3D formulation of the scalar depicting the isotropic damage
343 is given. By construction, u_d takes a the 3D aspect of the separation vec-
344 tor $\mathbf{u}$ into account and then $\dot{u}_d$ is non-negative and de facto respects the
345 irreversibility of the damage progress.

$$u_d = \ \max\{u_{eq}(\tau), \forall \tau \leqq t\} \ . \tag{26}$$

346 By definition, the state laws are the partial derivatives of the cohesive zone
347 potential *Eq.*(24). They introduce the components of the reversible traction
348 vector $\mathbf{f}^r$ and the conjugate variable A_d associated with (u_{t_1}, u_{t_2}, u_n) and u_d
349 respectively :

$$\begin{cases} f_n^r &= \frac{\partial \psi}{\partial u_n} &= K_n(u_d)u_n & & \\ f_{t_1}^r &= \frac{\partial \psi}{\partial u_{t_1}} &= \alpha K_n(u_d)u_{t_1} &= K_t(u_d)u_{t_1} \\ f_{t_2}^r &= \frac{\partial \psi}{\partial u_{t_2}} &= \alpha K_n(u_d)u_{t_2} &= K_t(u_d)u_{t_2} \\ A_d &= \frac{\partial \psi}{\partial u_d} &= \frac{1}{2}K'(u_d)u_{eq}^2 & \end{cases} . \tag{27}$$

Because only damage induces irreversibility, no dissipation has to be associated with the component of the separation vector. The reversible part $\mathbf{f}^r$ of the separation can therefore be identified with $\mathbf{f}$, then $\mathbf{f} = \mathbf{f}^r$.

3.2.1. Energy definition of the damage threshold

To extend our approach to an isotropic 3D CZM the evolution of the chosen damage variable, u_d, is directly linked to the evolution of the elastic energy w_e^d. This elastic energy, for a given damage state u_d, describes in the displacement space a half spheroid of radii $r_n = \left(\frac{2w_e^d}{k_n(ud)}\right)$ and $r_t = \left(\frac{2w_e^d}{\alpha\, k_n(ud)}\right) = \frac{r_n}{\alpha}$ as shown in Figure 4. As the normal jump denoted u_n is by definition positive or null only half of the spheroid is reachable for any separation states.

As long as the further separation states, $\mathbf{u}$, remain within the corresponding spheroid (i.e. $w_e(\mathbf{u}, u_d) \leq w_e^d(u_d)$), the behavior remains elastic. Then for a given opening such that $u_{eq} = u_d$, the elastic energy reaches the maximal value associated with this damage state (i.e. $w_e(\mathbf{u}, u_d) = w_e^d(u_d)$. Once the surface of the spheroid is reached :

— either the separation increment $\delta\mathbf{u}$ is directed towards the inside of the spheroid, and an elastic unloading at constant damage can be observed,

— or $\delta\mathbf{u}$ is directed towards the outside of the spheroid, and then the

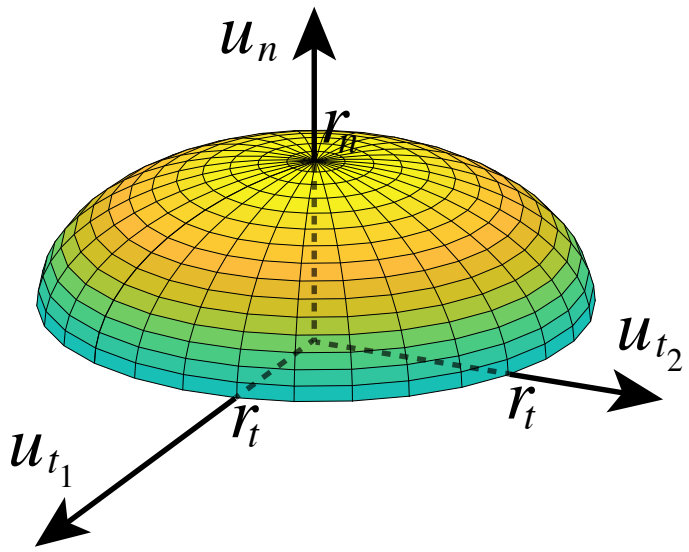

FIGURE 4: A 3D representation of the elastic energy allowable, $w_e^d(u_d)$, for a given damage state u_d . The color variation represents only the height U_n.

damage develops defining a new elastic limit surface.

For isotropic damage, a single evolution equation for u_d is required. We have already underlined that for threshold behavior law, the yield function depends on the thermodynamic forces and possibly on the states variables themselves, acting as parameters. In the present case, the thermodynamic force of the model , associated with the damage variable rate, is X_d. A generalized form of the yield criterion proposed in *Eq.*(22) is chosen where the role of u used in the 1D scenario is played by u_{eq}. So, the proposed yield criterion, derived of $\frac{d\,w_e^d}{dt}$, may be written as :

$$F(X_d; u_{eq}, u_d) = K_n(u_d)\, u_{eq} \;-\; X_d \;-\; \frac{d\,w_e^d}{d\,u_d}\;. \tag{28}$$

Damage develops if the threshold is reached, $F(X_d; u_{eq}, u_d) = 0$ and if the consistency condition is verified, $\dot{F}(X_d; u_{eq}, u_d) = 0$. For the same reasons as the ones shown for the 1D model, the evolution law of the parameter u_d is written as :

$$\dot{u}_d = \dot{u}_{eq} \text{ if } u_d = u_{eq} \text{ and } \dot{u}_{eq} \geq 0 \ , \tag{29}$$

results which, moreover, are imposed by the very definition of the damage variable.

An illustration of the energy criteria is given in Figure 5. Following a monotonic loading (i.e. remaining on the $w_e^d(u_d)$ curve), $K_n(u_d)u_d$ is the slope of the deformation energy w_{def}^d, X_d is the slope of the dissipated energy w_d^d and $(w_e^d)'$ is naturally the slope of the maximal allowable elastic energy w_e^d.

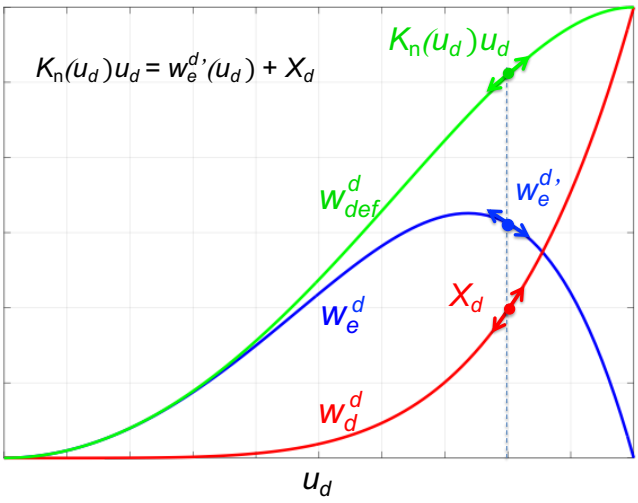

FIGURE 5: Illustration of the damage energy criterion - $u_{eq} = u_d$

To conclude section 3, we would like to stress once more the fact that

the damage threshold of is not here a matter of choice. It is imposed by the chosen form of the energy balance and by the definition of the damage state variable.

The state equations Eqs(27) and the evolution equation *Eq.*(29) will be, in what follows, implemented in a home-made finite element code. The different material parameter of the constitutive equations will be specified. In order to show the capabilities of such a CZM, simulations will be made and compared with some experimental results extracted from the literature.

4. Numerical Implementation

To illustrate the potentiality of the proposed model, simulations reproducing a common benchmark extracted from the literature [32][49] were carried out. It is important to notice that the objective of this practical comparison is simply to show the operability of the model and not to optimize its parameters in order to fit the benchmark. The numerical implementation of the previous model is then done in the code LMGc90 based on Non-Smooth Contact Dynamics (NSCD) [36; 37; 52]. The NSCD method is dedicated to solving problems related to dynamic systems with unilateral constraints. It is therefore particularly suitable for contact friction problems. It proposes a non-smooth treatment (no compliance, no penalty) of the conditions of contact [36], which is explicit in definition of u_n. The way which adhesion is taken into account in this method makes it possible to consider each point of contact as a cohesive zone. Then the mechanical behavior of the cohesive zones may vary at any point of the spatial discretization of the problem. This relevant modeling framework was then adopted to numerically simulate

crack propagation with cohesive zone [16] .

4.1. Benchmark

To compare the proposed model with a benchmark found in literature [32][49], the form of the maximum storable elastic energy, which we remember is $w_e^d(u_d)$, must be specified in order to be able to implement it in LMGc90 , the open source platform [1] used to carry out the simulations [28]. This benchmark, illustrated by Figure 6, traces the evolution of a crack in mixed mode to be followed. In the context of this feasibility study, a simple quadratic form of $w_e^d(u_d)$ is proposed. In what follows, we also assumed the existence of a pure elastic domain and thus the existence of a threshold equivalent elastic deplacement u_{eq}^e, simply denoted by u_e. The maximum storable elastic energy as a function of the damage parameter u_d simply reads :

$$w_e^d(u_d) \;=\; A\,(u_d - u_c)^2 + B\,(u_d - u_c)\,, \text{ if } u_e \leq u_d \leq u_c \quad , \tag{30}$$

where u_c is the critical equivalent displacement corresponding to the crack onset. Parameters A and B are two constants chosen to ensure the C_1 continuity of the maximum storable elastic energy, $w_e^d(u_d)$, at the threshold equivalent elastic deplacement, $w_e^d(u_e) = \frac{1}{2}\,K_n^0\,u_e^2$. They are defined by :

$$\left\{ \begin{array}{rcl} A & = & -\frac{1}{2}\,K_n^0\,u_e \frac{(2u_c - u_e)}{(u_c - u_e)^2} \\ B & = & -K_n^0 \frac{u_c u_e}{u_c - u_e} \end{array} \right. , \tag{31}$$

where K_n^0 is the initial normal stiffness of the CZM.

1. https ://git-xen.lmgc.univ-montp2.fr/lmgc90/

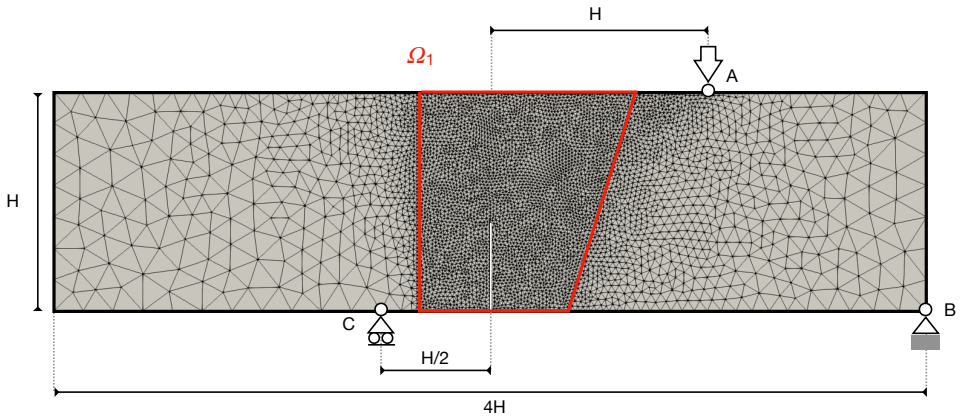

FIGURE 6: Characteristics of the benchmark issued from [32] used for simulation

The thickness of the sample, denoted by H, is equal to 0.3m while its length is equal to 1.2m. A 0.15m pre-crack is located in the middle on the lower edge. The point B is fixed in both x and y directions whereas the point A is only fixed in the y direction. A displacement is imposed on the point A to load the structure. The mesh is composed of 3 parts : Two continuous meshes (the left and the right parts of the structure) composed respectively of 958 and 2 063 T3 elements and 6 723 meshes composed of a single T3 element assuring the continuity of the structure (domain Ω_1 on Figure 6). The interactions between elements of Ω_1 are governed by the proposed cohesive zone model where the initial secant elastic stiffness, K_n^0 and K_t^0, are chosen to satisfy the criterion proposed in [9] to limit the reduction of stiffness due to the presence of CZM. It is important to underline that the objective of this practical comparison is simply to show the operability of the model and not to optimize its parameters in order to fit the benchmark. The values of the CZM parameters are summarized in Table 1.

Figure 7 shows the evolution, for different simulation times, of different

K_n^0 (N/m)	α	u_e (m)	u_c (m)
$2.48\ 10^9$	0.5	$0.5\ 10^{-6}$	$1.5\ 10^{-6}$

TABLE 1: Parameter values of the CZM

characteristic quantities associated with the model : the damage variable, the elastic energy w_e and the dissipated energy w_d. In order to present a quantity varying from 0 to 1 the damage ratio, as a function the damage variable, is introduced and defined by $\frac{<u_d-u_e>^+}{u_c-u_e}$. To improve the visibility of these different quantities supported by the interfaces, they are projected on adjacent elements.

Figure 7(a), corresponding to a pre-cracking state, shows a concentration of the elastic energy at the outset of the crack tip. However, the damage criterion has not been reached within the cohesive zone so that no damage or dissipation has yet occurred (see *Eq.*(17)). The corresponding map to $\frac{<u_d-u_e>^+}{u_c-u_e}$ and w_d are then uniformally egal to 0. As expected, Figure 7 (b) and (c), corresponding to two post-cracking steps, highlight the correlation between the evolution of the dissipated energy and the damage ratio. The elastic energy is still concentrated ahead of the crack tip, then returns to zero along the crack lips. In contrast, the dissipated energy related to the damage evolution can be exhibited all along the crack path. Similarly, the damage field allows the cracking path to be tracked.

To exhibit the capability of our CZM where only the shape of the cohesive energy associated with a simple energy balance is needed (cf. *Eq.*(30)), different quantities, numerically obtained, are compared with experimental

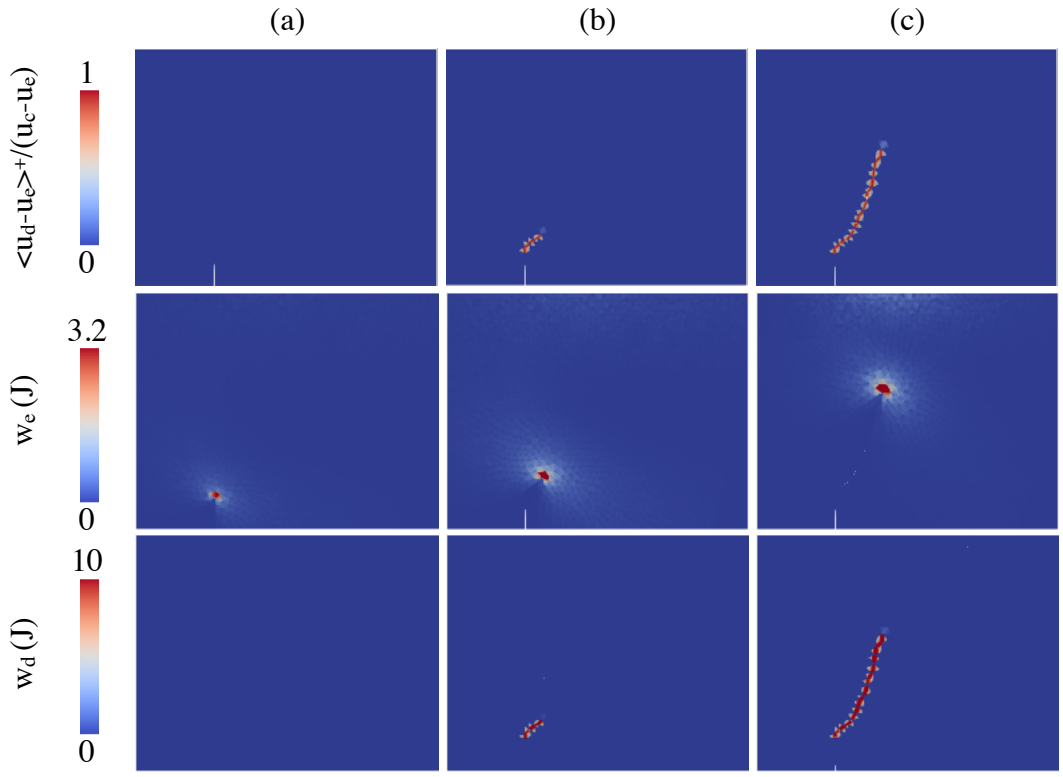

FIGURE 7: Visualization of the damage ratio (top row), the elastic energy (center) and the dissipated energy (bottom row) during the crack propagation

measurements present in the literature [14]. For such comparisons, Figure 8 presents both the classical crack path monitoring and the load vs. CMOD curve (Crack Mouth Opening Displacement).

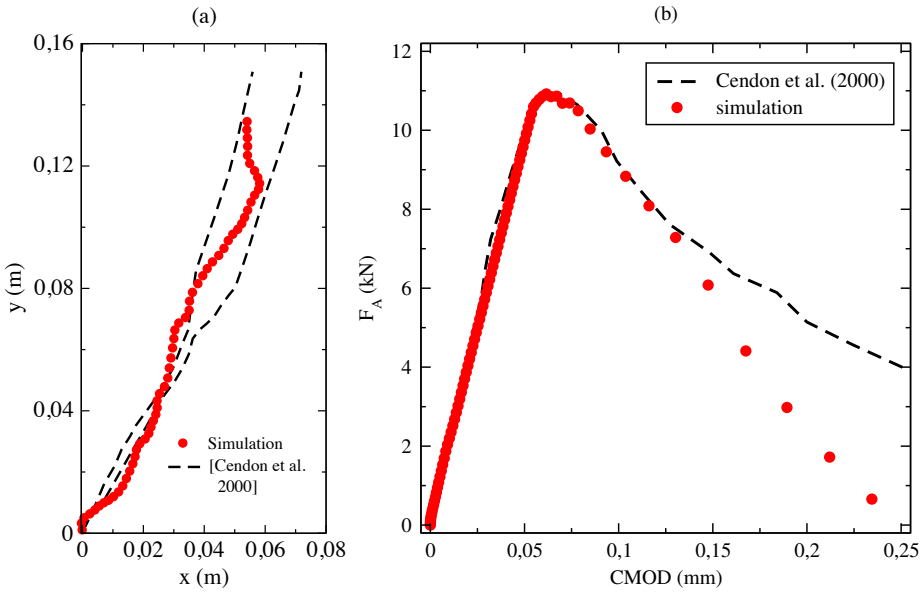

FIGURE 8: Comparison of numerical macroscopic measurements associated to the crack evolution with experimental results [14] : a) The crack path and b) the load vs. CMOD curve.

In Figure 8(a) and Figure 8(b), the red dot line corresponds to the simulation result while the black dashed lines represent the crack envelop obtained experimentally [14]. In Figure 8a, the crack obtained numerically corresponds closely to the experimental envelope. The starting angle is strongly related to the discretization around the initiation point, explaining the slight difference at the beginning of the initiation. Then, the path is corrected and repositioned in the experimental envelope until the end of the simulation.

Concerning the force vs. CMOD curves, they fit perfectly in the section

corresponding to the linear increase. This highlight that the introduction of a 2D interface element, where the values of K_n^0 and K_t^0 satisfy the criterion proposed in [9] between each elements of Ω_1 do not affect the global stiffness of the sample. The maximum force obtained is also in good agreement with that obtained in the experiment, as well as the beginning of the non-linear decreasing part of the CMOD curve occurring at the initiation of cracking. In the last part, the curves diverge. This difference is partly explained by the fact that the numerical simulation is two-dimensional while the experiments are three-dimensional. Indeed, not all deformation modes are taken into account (especially out-of-plane modes), which explains this different behavior at the end of the simulation. Moreover, we have arbitrarily chosen a 2nd degree polynomial to characterize the damage of the cohesive zone model, *Eq.*(30). This choice could be fine-tuned in order to better account for experiences by taking a Needleman-type damage, [26; 54].

4.2. Sensitivity study

Finally, in order to see the impact of a variation in the parameters u_e and u_c on the overall behavior of the system and more particularly on the evolution of the force vs. CMOD curves, a sensitivity study is proposed. The influence of these parameters on the crack path is not presented because it is not very significant. The influence of these parameters on the energy available to be dissipated in the model is pointed out in Figure 9. The parametric study is carried out relative to the reference point $(0, 0)$ corresponding to the results presented on the Figure 8(b) with the parameters define in table 1. With the chosen law, a variation of u_c has almost the same consequence as a variation of u_e in terms of the energy available to be dissipated. Then the

map presented on Figure 9 is symmetric in the regard of the circle-triangle diagonal. During the different parametric studies, the color code used for the curves will refer to the one defined in the Figure 9.

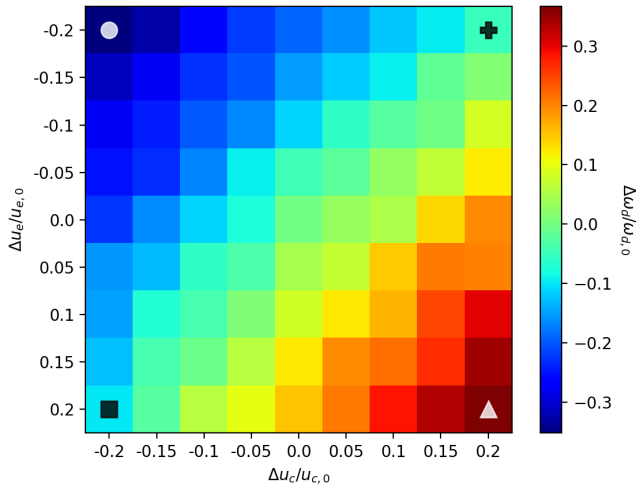

FIGURE 9: Map of the normalized dissipated energy variations as a function of the variations of u_e and u_c. The symbols used at the four corners of the map identify the curves shown in Figure 10.

The Figure 10 presents the normalized plots of $w_e^d(u_d)$ for different values of u_e and u_c (Figure 10(a)) and the corresponding force vs. CMOD curves (Figure 10(b)). The normalization parameters are $u_{e,0} = 0.5\,10^{-2}$ and $w_{e,0} = w_{e,0}^d(u_{e,0})$ using the values of parameters in Tab. 1. Even if the shape of the curves is significantly different in Figure 10 (a), the energies available to be dissipated for the case represented by a cross and the one represented by a square are of same order of magnitude. The maxima order observed at the scale of the CZM models (Figure 10(a)) is conserved at the scale of the structure (Figure 10(b)).

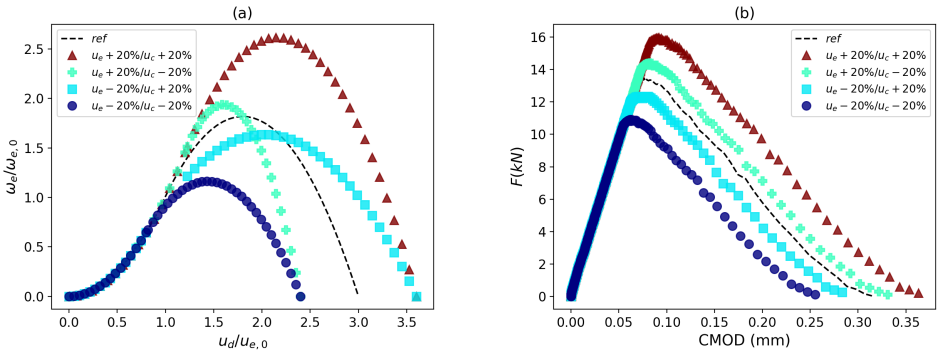

FIGURE 10: (a) Normalized plots of $w_e^d(u_d)$ for different values of u_e and u_c. The normalization parameters are $u_{e,0} = 0.5\,10^{-2}$ and $w_{e,0} = w_{e,0}^d(u_{e,0})$ using the values of parameters in Tab.1. (b) Corresponding force vs. CMOD curves.

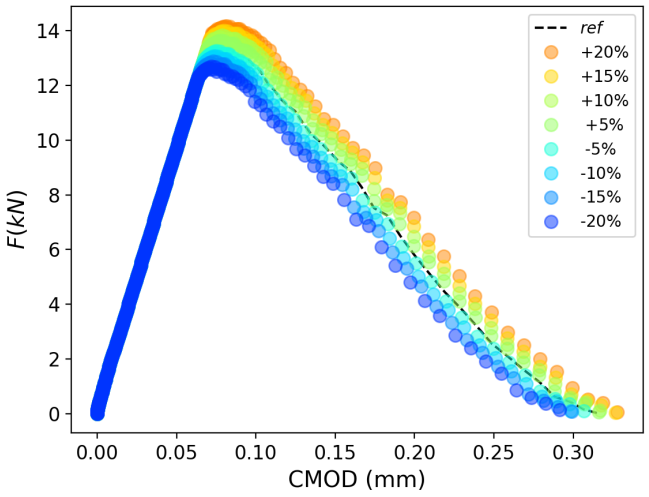

FIGURE 11: Comparison between the reference Load vs. CMOD curve (dash line) and the ones related to the variation of u_c of $\pm 20\%$ while u_e constant.

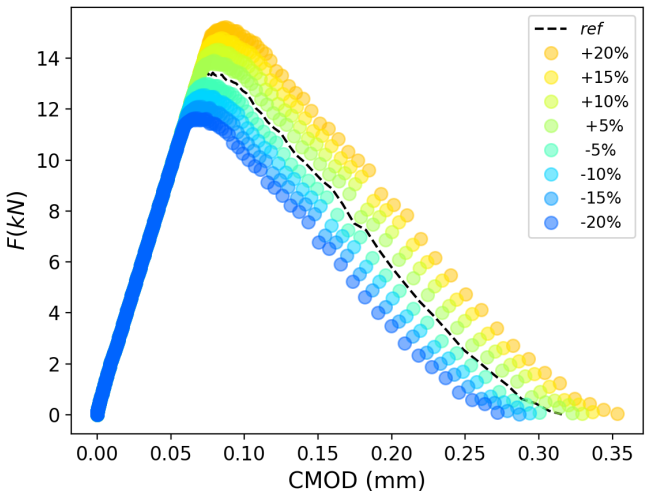

FIGURE 12: Comparison between the reference Load vs. CMOD curve (dash line) and the ones related to the variation of u_e of $\pm 20\%$ while u_c constant.

On figures Figure 11 to Figure 13, we observe respectively the influence of u_c and u_e on the force vs. CMOD curves. These figures show that the influence of the variation of u_c is less than that of u_e. Indeed, where we observe for a variation of u_c a variation of less than 10% on the critical values of the curve (F_{max} and $CMOD_{max}$), while a variation of more than 20% for an equivalent variation of u_e is observed. Nevertheless, in both cases, an increase of the damage energy w_d induces an increase of the CMOD and loading maxima in the Load vs. CMOD curve. In this model where an elastic domain is assumed, u_e is the threshold where the damage begins to occur. This value determines the outset of the non-linear response of the structure. This is exhibited in Figure 12 where an increase of u_e at the local scale induces an increase of the maximal force at the macroscopic scale and a delay of the occurence of the nonlinear response of the curves.

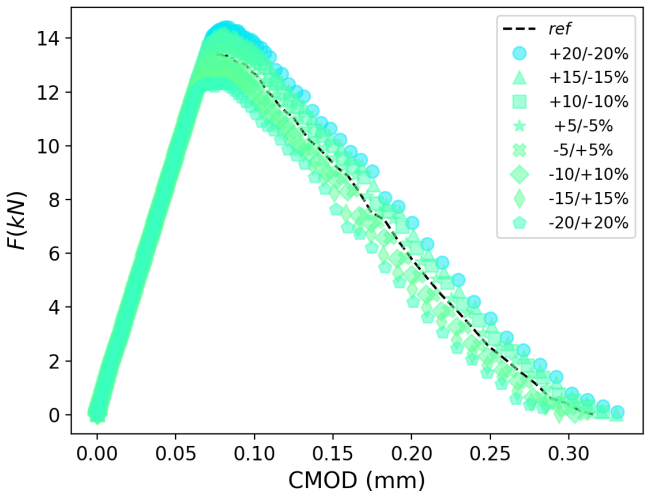

FIGURE 13: Comparison between the reference Load vs. CMOD curve (dash line) and the ones related to the variation of u_c and u_e of $\pm 20\%$ W constant.

Figure 13 demonstrates that the non-linear region of the curve is also governed by the shape of the energy curve (cf. Figure 10). Although the dissipative energy in this parametric study is almost constant, we observe a variation of about 10% on the characteristic values of the response curve. So by combining the effects of u_e, u_c and the shape of the local curve (cf. Figure 10) it is possible to obtain a better optimal result to fit experiments. Thus the experimental characterization of this type of local curve depicting the micro-structural phenomenon linked to fracture is relevant and is still an ongoing problem.

5. Conclusion

In this paper we present an energy criterion for cohesive zone models where the damage progress is assessed together with the ability of the ma-

terial to store energy elastically. The damage parameter used is $u_d(t) = Sup\{u_{eq}(\tau), \tau \leq t\}$ where u_{eq} is an equivalent strain compatible with the isotropic evolution of the damage progress. The cohesive zone law is then completely defined through the function $w_e^d(u_d)$ which represents the maximum elastic energy which can be stored in the material for a given damage state associated with a simple energy balance. The identification of the function, $w_e^d(u_d)$ will be based on the analysis of the experimentally derived energy balance associated with the material transformations, in addition to the kinematic aspects near the crack tip, the dissipative effects accompanying the damage progress, inducing temperature variations at the crack tip. The thermodynamic coherence of the proposed model effectively makes it possible to directly relate damage and temperature. We have implemented the chosen model in the code LMGc90 based on Non-Smooth Contact Dynamics (NSCD) and performed numerical simulations in the case of a bending test. The results obtained for this 2-D modeling are encouraging. Using a simple quadratic function $w_e^d(u_d)$ for the interface, we obtained a close correlation between the simulations and the experimental observations of the crack path. A first parametric study of the macroscopic response of the structure naturally demonstrates the importance of the shape of the function $w_e^d(u_d)$ which characterize the interface behavior between two elements. In subsequent developments, we will consider high cycle fatigue in cohesive zone models while preserving this framework to define and quantify damage. An extension to investigate the non isotropic degradation of a material to store elastic energy could also be envisaged.

Références

[1] Abdelmoula, R., Marigo, J.-J., Weller, T., 2009. Construction des lois de fatigue à partir de modèleles de forces cohésivesives : cas de fissures en mode i. Comptes Rendus Mécanique 337 (3), 166 – 172.
URL http://www.sciencedirect.com/science/article/pii/S1631072109000382

[2] Alessi, R., Jul. 2013. Variational approach to fracture mechanics with plasticity. Theses, Ecole Polytechnique X.
URL https://pastel.archives-ouvertes.fr/pastel-00847970

[3] Alessi, R., Marigo, J.-J., Vidoli, S., 2015. Gradient damage models coupled with plasticity : Variational formulation and main properties. Mechanics of Materials 80 (Part B), 351 – 367, materials and Interfaces.
URL http://www.sciencedirect.com/science/article/pii/S0167663614000039

[4] Allix, O., Ladevèze, P., Corigliano, A., 1995. Damage analysis of interlaminar fracture specimens. Composite Structures 31 (1), 61 – 74.
URL http://www.sciencedirect.com/science/article/pii/026382239500002X

[5] Amor, H., Marigo, J.-J., Maurini, C., 2009. Regularized formulation of the variational brittle fracture with unilateral contact : Numerical experiments. Journal of the Mechanics and Physics of Solids 57 (8), 1209 – 1229.

URL http://www.sciencedirect.com/science/article/pii/S0022509609000659

[6] B., H., Q.S., N., 1975. Sur les matériaux standards generalisés. Journal de mécanique 14, 39,63.

[7] Barrenblatt, G., 1962. The mathematical theory of equilibrium of cracks in brittle fracture. Adv. Appl. Mech. 7, 55–129.

[8] Bernard, P., Moës, N., Chevaugeon, N., 2012. Damage growth modeling using the thick level set (tls) approach : Efficient discretization for quasi-static loadings. Computer Methods in Applied Mechanics and Engineering 233-236, 11 – 27.
URL http://www.sciencedirect.com/science/article/pii/S004578251200062X

[9] Blal, N., Daridon, L., Monerie, Y., Pagano, S., 2011. Criteria on the artificial compliance inherent to the intrinsic cohesive zone. Comptes Rendus Mécanique 339 (12), 789 – 795.
URL http://www.sciencedirect.com/science/article/pii/S1631072111001677

[10] Blaysat, B., Hoefnagels, J., Lubineau, G., Alfano, M., Geers, M., 2015. Interface debonding characterization by image correlation integrated with double cantilever beam kinematics. International Journal of Solids and Structures 55 (Supplement C), 79 – 91, special Issue Computational and Experimental Mechanics of Advanced Materials A workshop held at King Abdullah University of Science and Technology Jeddah, Kingdom

of Saudi Arabia July 1-3, 2013.
URL http://www.sciencedirect.com/science/article/pii/S0020768314002443

[11] Bouvard, J., Chaboche, J., Feyel, F., Gallerneau, F., 2009. A cohesive zone model for fatigue and creep-fatigue crack growth in single crystal superalloys. International Journal of Fatigue 31 (5), 868 – 879.
URL http://www.sciencedirect.com/science/article/pii/S0142112308002521

[12] Brocks, W., Cornec, A., Scheider, I., july 2003. Computational aspects of nonlinear fracture mechanics. Technical Report - GKSS-Forschungszentrum Geesthacht GmbH (Germany) 3, 127–209.

[13] Cazes, F., Moës, N., July 2015. Comparison of a phase-field model and of a thick level set model for brittle and and quasi-brittle fracture. Numerical Methods in Engineering 103 (2), 114–143.

[14] Cendón, D., Gálvez, J., Elices, M., Planas, J., Jun 2000. Modelling the fracture of concrete under mixed loading. International Journal of Fracture 103 (3), 293–310.
URL https://doi.org/10.1023/A:1007687025575

[15] Chaboche, J., Feyel, F., Monerie, Y., 2001. Interface debonding models : a viscous regularization with a limited rate dependency. International Journal of Solids and Structures 38 (18), 3127 – 3160.
URL http://www.sciencedirect.com/science/article/pii/S0020768300000536

[16] Champagne, M., Renouf, M., Berthier, Y., 01 2014. Modeling Wear for Heterogeneous Bi-Phasic Materials Using Discrete Elements Approach. Journal of Tribology 136 (2), 021603.
URL https://doi.org/10.1115/1.4026053

[17] Chen, Z., Bunger, A., Zhang, X., Jeffrey, R. G., 2009. Cohesive zone finite element-based modeling of hydraulic fractures. Acta Mechanica Solida Sinica 22 (5), 443 – 452.
URL http://www.sciencedirect.com/science/article/pii/S0894916609602950

[18] Chrysochoos, A., 2012. Infrared thermography applied to the analysis of material behavior : a brief overview. Quantitative InfraRed Thermography Journal 9 (2), 193–208.
URL https://doi.org/10.1080/17686733.2012.746069

[19] Chrysochoos, A., 2012. Thermomechanical analysis of the cyclic behavior of materials. Procedia IUTAM 4, 15 – 26, iUTAM Symposium on Full-field Measurements and Identification in Solid Mechanics.
URL http://www.sciencedirect.com/science/article/pii/S2210983812000272

[20] Chrysochoos, A., Daridon, L., Wattrisse, B., Jul. 2014. Prediction of damage evolution in bonded material using cohesive zone model. In : 11th World Congress on Computational Mechanics - 5th European Conference on Computational Mechanics. Barcelone, Spain.
URL https://hal.archives-ouvertes.fr/hal-01103157

[21] Corigliano, A., 1993. Formulation, identification and use of interface models in the numerical analysis of composite delamination. International Journal of Solids and Structures 30 (20), 2779 – 2811.
URL http://www.sciencedirect.com/science/article/pii/002076839390154Y

[22] Corigliano, A., Allix, O., 2000. Some aspects of interlaminar degradation in composites. Computer Methods in Applied Mechanics and Engineering 185 (2), 203 – 224.
URL http://www.sciencedirect.com/science/article/pii/S0045782599002601

[23] Corigliano, A., Ricci, M., 2001. Rate-dependent interface models : formulation and numerical applications. International Journal of Solids and Structures 38 (4), 547 – 576.
URL http://www.sciencedirect.com/science/article/pii/S0020768300000883

[24] Daridon, L., Cochelin, B., Ferry, M. P., 1997. Delamination and fiber bridging modelling in composite samples. Journal of Composite Materials 31 (9), 874–888.
URL https://doi.org/10.1177/002199839703100902

[25] Daridon, L., Wattrisse, B., Chrysochoos, A., Potier-Ferry, M., 2011. Solving fracture problems using an asymptotic numerical method. Computers & Structures 89 (5), 476 – 484.
URL http://www.sciencedirect.com/science/article/pii/S0045794910002841

[26] den Bosch, M. V., Schreurs, P., Geers, M., 2006. An improved description of the exponential xu and needleman cohesive zone law for mixed-mode decohesion. Engineering Fracture Mechanics 73 (9), 1220 – 1234.
URL http://www.sciencedirect.com/science/article/pii/S0013794406000026

[27] Dubois, F., Jean, M., 2006. The non smooth contact dynamic method : recent LMGC90 software developments and application. Springer Berlin Heidelberg, Berlin, Heidelberg, pp. 375–378.
URL https://doi.org/10.1007/3-540-31761-9_44

[28] Dubois, F., Jean, M., Renouf, M., Mozul, R., Martin, A., Bagnéris, M., May 2011. LMGC90. In : 10e colloque national en calcul des structures. Giens, France, p. Clé USB.
URL https://hal.archives-ouvertes.fr/hal-00596875

[29] Dugdale, D., 1960. Yielding of steel sheets containing slits. Journal of the Mechanics and Physics of Solids 8 (2), 100 – 104.
URL http://www.sciencedirect.com/science/article/pii/0022509660900132

[30] Fremond, M., 2002. Non-smooth Thermomechanics. Springer-Verlag Berlin Heidelberg.

[31] Gálvez, J., Elices, M., Guinea, G., Planas, J., december 1998. Mixed mode fracture of concrete under proportional and nonproportional loading. International Journal of Fracture 94 (3), 267–284.

[32] Galvez, J., Elices, M., Guinea, G. V., Planas, J., Jun 1996. Crack trajectories under mixed mode and non-proportional loading. International Journal of Fracture 81 (2), 171–193.
URL https://doi.org/10.1007/BF00033181

[33] Giulio, A., May 2006. On the influence of the shape of the interface law on the application of cohesive-zone models. Composites Science and Technology 66 (6), 723–730.
URL http://www.sciencedirect.com/science/article/B6TWT-4FF8WMX-2/2/ee8b268696a03502b511be734dd46694

[34] Giulio, A., Elio, S., 10 2006. Combining interface damage and friction in a cohesive, zone model. International Journal for Numerical Methods in Engineering 68 (5), 542–582.
URL http:https://doi.org/10.1002/nme.1728

[35] Huon, V., Richefeu, V., Shuang, W., Chrysochoos, A., Monerie, Y., Wattrisse, B., 2010. Experimental characterisation of a cohesive zone model using digital image correlation. EPJ Web of Conferences 6, 43004.
URL https://doi.org/10.1051/epjconf/20100643004

[36] Jean, M., 1999. The non-smooth contact dynamics method. Computer Methods in Applied Mechanics and Engineering 177 (3), 235 – 257.
URL http://www.sciencedirect.com/science/article/pii/S0045782598003831

[37] Jean, M., Acary, V., Monerie, Y., 2001. Non-smooth contact dynamics approach of cohesive materials. Philosophical Transactions of the Royal

Society of London A : Mathematical, Physical and Engineering Sciences 359 (1789), 2497–2518.
URL http://rsta.royalsocietypublishing.org/content/359/1789/2497

[38] Julian Rimoli, J. R., Khemani, F., 2012. On the mesh dependency of cohesive zone models for crack propagation analysis. In : 53rd AIAA/ASME/ASCE/AHS/ASC Structures, Structural Dynamics and Materials Conference - Honolulu, Hawaii.

[39] Kachanov, L., 1986. Introduction to continuum damage mechanics. springer.

[40] Kolluri, M., Hoefnagels, J. P. M., Samimi, M., van Dommelen, H., van der Sluis, O., Geers, M. G. D., 2012. An in situ experimental-numerical approach for characterization and prediction of interface delamination : Application to culf-mce systems. Advanced Engineering Materials 14 (11), 1034–1041.
URL http://dx.doi.org/10.1002/adem.201200110

[41] Kolluri, M., Hoefnagels, J. P. M., van Dommelen, J. A. W., Geers, M. G. D., Sep 2013. A practical approach for the separation of interfacial toughness and structural plasticity in a delamination growth experiment. International Journal of Fracture 183 (1), 1–18.
URL https://doi.org/10.1007/s10704-013-9871-y

[42] Kolluri, M., Hoefnagels, J. P. M., van Dommelen, J. A. W., Geers, M. G. D., Jan 2014. Irreversible mixed mode interface delamination using

a combined damage-plasticity cohesive zone enabling unloading. International Journal of Fracture 185 (1), 77–95.
URL https://doi.org/10.1007/s10704-013-9899-z

[43] Kondo, D., Welemane, H., Cormery, F., 2007. Basic concepts and models in continuum damage mechanics. Revue Européenne de Génie Civil 11 (7-8), 927–943.
URL https://doi.org/10.1080/17747120.2007.9692970

[44] Kuna, M., Roth, S., 2015. General remarks on cyclic cohesive zone models. International Journal of Fracture 196 (1), 147–167.
URL https://doi.org/10.1007/s10704-015-0053-y

[45] Lé, B., Moës, N., Legrain, G., 2018. Coupling damage and cohesive zone models with the thick level set approach to fracture. Engineering Fracture Mechanics 193, 214 – 247.
URL http://www.sciencedirect.com/science/article/pii/S0013794417312523

[46] Lemaitre, J., 1996. A course on dammage mechanics. springer.

[47] Lorentz, E., Andrieux, S., 1999. A variational formulation for nonlocal damage models. International Journal of Plasticity 15 (2), 119 – 138.
URL http://www.sciencedirect.com/science/article/pii/S0749641998000576

[48] Marigo, J.-J., Maurini, C., Pham, K., Dec 2016. An overview of the modelling of fracture by gradient damage models. Meccanica 51 (12),

3107–3128.
URL https://doi.org/10.1007/s11012-016-0538-4

[49] Moës, N., Belytschko, T., 2002. Extended finite element method for cohesive crack growth. Engineering Fracture Mechanics 69 (7), 813 – 833.
URL http://www.sciencedirect.com/science/article/pii/S001379440100128X

[50] Moës, N., Stolz, C., Bernard, P.-E., Chevaugeon., N., 4 2011. A level set based model for damage growth : The thick level set approach. International Journal for Numerical Methods in Engineering 86 (3), 358–380.
URL http:https://doi.org/10.1002/nme.3069

[51] Moës, N., Stolz, C., Parrilla-Gomez, A., 2015. Passage du modèle d'endommagement thick level set au modèle de zone cohésive et vice versa : cas unidimensionnel. In : 12e Colloque national en calcul des structures.

[52] Moreau, J. J., 1988. Unilateral Contact and Dry Friction in Finite Freedom Dynamics. Springer Vienna, Vienna, pp. 1–82.
URL https://doi.org/10.1007/978-3-7091-2624-0_1

[53] Needleman, A., 1987. A continuum model for void nucleation by inclusion debonding. Journal of applied mechanics 54, 525–531.

[54] Needleman, A., 1990. An analysis of tensile decohesion along an interface. Journal of the Mechanics and Physics of Solids 38 (3), 289 – 324.

URL http://www.sciencedirect.com/science/article/pii/002250969090001K

[55] Nguyen, O., Repetto, E., Ortiz, M., Radovitzky, R., Aug 2001. A cohesive model of fatigue crack growth. International Journal of Fracture 110 (4), 351–369.
URL https://doi.org/10.1023/A:1010839522926

[56] Onsager, L., Feb 1931. Reciprocal relations in irreversible processes. i. Phys. Rev. 37, 405–426.
URL https://link.aps.org/doi/10.1103/PhysRev.37.405

[57] Ortiz, M., Pandolfi, A., 1999. Finite-deformation irreversible cohesive elements for three-dimensional crack-propagation analysis. International journal of numerical method in engineering. 44 (9), 1267–1282.

[58] Pandolfi, A., Ortiz, M., 2003. A cohesive model for fatigue crack. In : Acta Fracturae , Atti convegni Nazionali IGF ISSN : 2281-1443.

[59] Pandolfi, A., Ortiz, M., novembre 2013. Modeling fracture by material-point erosion. International Journal of Fracture 184 (1-2), 3–16.

[60] Park, K., Paulino, G. H., Roesler, J. R., 2009. A unified potential-based cohesive model of mixed-mode fracture. Journal of the Mechanics and Physics of Solids 57 (6), 891 – 908.
URL http://www.sciencedirect.com/science/article/pii/S0022509608001713

[61] Pham, K., Marigo, J.-J., 2010. Approche variationnelle de l'endommagement : Ii. les modèles à gradient. Comptes Rendus Mécanique

338 (4), 199 – 206.
URL http://www.sciencedirect.com/science/article/pii/S1631072110000446

[62] Pham, K., Marigo, J.-J., 2012. Damage localization and rupture with gradient damage models. Fracture and structural integrity 19, 5–19.

[63] Pijaudier-Cabot, G., Bazant, Z. P., 1987. Nonlocal damage theory. Journal of Engineering Mechanics 113 (10), 1512–1533.

[64] Richefeu, V., Chrysochoos, A., Huon, V., Monerie, Y., Peyroux, R., Wattrisse, B., 2012. Toward local identification of cohesive zone models using digital image correlation. European Journal of Mechanics - A/Solids 34 (Supplement C), 38 – 51.
URL http://www.sciencedirect.com/science/article/pii/S0997753811001690

[65] Roe, K., Siegmund, T., 2003. An irreversible cohesive zone model for interface fatigue crack growth simulation. Engineering Fracture Mechanics 70 (2), 209 – 232.
URL http://www.sciencedirect.com/science/article/pii/S0013794402000346

[66] Roth, S., Hütter, G., Kuna, M., Jul 2014. Simulation of fatigue crack growth with a cyclic cohesive zone model. International Journal of Fracture 188 (1), 23–45.
URL https://doi.org/10.1007/s10704-014-9942-8

[67] Roy, Y. A., Dodds, R. H., 2001. Simulation of ductile crack growth in thin aluminum panels using 3-d surface cohesive elements. International Journal of Fracture 110 (1), 21–45.
URL https://doi.org/10.1023/A:1010816201891

[68] Serpieri, R., Sacco, E., Alfano, G., 2015. A thermodynamically consistent derivation of a frictional-damage cohesive-zone model with different mode i and mode ii fracture energies. European Journal of Mechanics - A/Solids 49, 13 – 25.
URL http://www.sciencedirect.com/science/article/pii/S0997753814000837

[69] Suo, Z., Hutchinson, J. W., May 1990. Interface crack between two elastic layers. International Journal of Fracture 43 (1), 1–18.
URL https://doi.org/10.1007/BF00018123

[70] Wojtacki, K., Daridon, L., Dubois, F., Moës, N. N., Monerie, Y., May 2015. Analyse comparative de trois méthodes performantes de simulation numérique de la fissuration. 13e colloque national en calcul des structures - CSMA.

[71] Zener, C., Jan 1938. Internal friction in solids ii. general theory of thermoelastic internal friction. Phys. Rev. 53, 90–99.
URL https://link.aps.org/doi/10.1103/PhysRev.53.90

[72] Zhang, X., Liu, H.-Y., Mai, Y.-W., 2003. Rate-dependent bridging law and its application to dynamic crack growth in brittle-matrix composite materials. Composites Part A : Applied Science and Manufacturing

34 (11), 1053 – 1063.
URL http://www.sciencedirect.com/science/article/pii/S1359835X03002355

[73] Zhang, X., Mai, Y.-W., Jeffrey, R. G., 2003. A cohesive plastic and damage zone model for dynamic crack growth in rate-dependent materials. International Journal of Solids and Structures 40 (21), 5819 – 5837.
URL http://www.sciencedirect.com/science/article/pii/S0020768303003706

[74] Zhou, F., Molinari, J. F., 2004. Dynamic crack propagation with cohesive elements : a methodology to address mesh dependency. International Journal for Numerical Methods in Engineering 59 (1), 1–24.
URL https://onlinelibrary.wiley.com/doi/abs/10.1002/nme.857